Original Research Article

Study of Solar Wind Parameters During Geomagnetic Storm of 26th August 2018 and 28th September 2017

Ashok Silwal[1], Sujan Prasad Gautam[2,*], Keshab Chaudhary[3], Manish Khanal[4], Sandip Joshi[3], Sanjay Dangaura[3], Binod Adhikari[5]

[1]Patan Multiple Campus, Tribhuvan University, Lalitpur, NEPAL

[2]Central Department of Physics, Tribhuvan University, Kirtipur, NEPAL

[3]Department of Physics, Kailali Multiple Campus, Tribhuvan University, Dhangadi, NEPAL

[4]Amrit Campus, Tribhuvan University, Kathmandu, NEPAL

[5]Department of Physics, St. Xavier College, Maitighar, Kathmandu, NEPAL

[*]Corresponding author E-mail: astrosujan@gmail.com

Received: 14th February 2021, Revised: 28th April 2021, Accepted: 30th April 2021

Abstract

In this paper, we have studied solar wind parameters, interplanetary magnetic field (B), solar wind speed (Vsw), solar wind density (Nsw), solar wind temperature (Tsw), and the south-north components of magnetic field Bz, By and Bx and geomagnetic index, SYM-H during the geomagnetic event of 27th – 29th September 2017 and 25th – 27th August 2018 using OMNI data. These parameters play a vital role in a better understanding of geomagnetic storms. The selection of the events has been made by using the equatorial index, the SYM-H index. In our work, during the moderate geomagnetic event of 27th-29th September 2017, we observed a sudden change in the magnetic field, which is evident from the minimum value of Bz (-8 nT). With the SYM-H index, we noticed sudden commencement around 00:30 UT, and it falls to a minimum value (-74 nT) with a couple of local minima. Similarly, during the intense geomagnetic event of 25th – 27th August 2018, Bz turns northward, reaching a value of -16.22 nT, and the SYM-H index decreased and reached the minimum value of -206 nT, and the Bz changed its polarity several times at different phases of the storm. For more illustration, we have used cross-correlation and wavelet analysis techniques. Cross-correlation analysis presented the strong negative association of SYM-H with Vsw, Nsw, Tsw, By, and B at a 0-min time lag. On the other hand, SYM-H shows a strong positive correlation with Bx at zero-time lag, and for Bz, it shows poor association with a very low correlation coefficient. Moreover, the CWT has revealed to be an effective tool in the time localization of the interplanetary magnetic field component (Bz) parameters,

and it may be the most convenient to represent times series with abrupt variations or steps, i.e., very small and localized variations as the discontinuities in the provided signal used for the study.

Keywords: Solar wind, Geomagnetic storms, SYM-H, Cross-correlation, Wavelet analysis

Introduction

Coronal mass ejections (CMEs) are solar coronal phenomena in which a massive amount of plasma is expelled. CMEs enclose a cluster of plasma, ions, electrons, and other solar particles, all of which are encased in a massive amount of energy [1]. The combined influence of the plasma's radial outward motion and the rotational motion of the sun causes the plasma to travel radially outward. This also causes the magnetic lines to become spiral in shape [1,2].

The solar wind is a stream of energized plasma containing charged particles, mainly protons, and electrons, flowing outward from the sun through the solar system at about a speed of 400 km/s and a temperature of 10^6 K [3]. The sun releases approximately 100 tons of solar wind every day, containing a large amount of kinetic and electrical energy. Among these energies, some enter directly into the Earth's magnetosphere, which causes heating of the Earth; ultimately, these energies enter the magnetosphere. As a result, the geomagnetic activity gets disturbed, which results in different phenomena as geomagnetic storms, sub-storms, and aurora [4-6]. The region where Earth's magnetic field is dominant called the magnetosphere, which is formed due to interaction among charged particles coming from the sun and Earth's magnetic field, and the shape of Earth's magnetosphere, which is determined by the solar wind, prevents most of the particles coming from the sun (which are carried by the solar wind) from hitting the Earth [7]. The two essential parameters of the solar wind are the dynamic pressure of the solar wind (which depends on its velocity and density). The dawn-dusk component of the interplanetary electric field (IEF), the increase in dynamic pressure, causes compression in the magnetosphere and magnetic field of solar wind or interplanetary magnetic field (IMF) interact with the Earth's magnetic field to facilitate the transfer of an increased amount of energy into the magnetosphere [7]. These interactions cause an increase in the mobility of plasma through the magnetosphere and an increase in electric current in the magnetosphere and ionosphere [6], which causes geomagnetic disturbance [7].

Disturbance storm time index (Dst) and Symmetric H-component (SYM-H) are the two geomagnetic indices, which primarily represent ring current intensity during geomagnetic storms, and these are obtained by using the longitudinally disturbing chain of low latitude ground-based magnetometers [8]. SYM-H and Dst are similar, but SYM-H has a 1-minute temporal resolution, which is very useful for studying short temporal variations during the geomagnetic storm [9].

A geomagnetic storm is an interval of time in which a sufficiently intense and long-lasting interplanetary convection electric field heads, through a substantial energization in the magnetosphere and ionosphere system, to an intensified ring current, which is strong enough to overcome some

key threshold of the quantifying storm time Dst index [10,11]. According to Adhikari et al. [12], Kp (logarithmic), Ap (linear), Dst (disturbance storm time), and geomagnetic AE and AL (auroral electrojet) indices are the determining factors to discover, study, and for the analysis of magnetic storms, sub-storms, and super substorms. The geomagnetic storms are divided into four categories depending on the value of Dst as suggest as weak or small (-30 nT to -50 nT); moderate (-50 nT to -100 nT); intense (-100 nT to -250 nT) and very intense (-250 nT and above) [11-13].

The interplanetary magnetic field (IMF) orientated southward can reconnect with the geomagnetic field of the dayside magnetosphere [7], resulting in the storage of energy in the lobes of the magnetotail [14]. Reconnection associated with disturbances in the magnetotail current sheet releases the stored energy. As a result, the upper atmosphere currents are increased, leading to adverse effects in-ground- and space-based technologies, the health of astronauts, and flight crew and passengers [15]. In particular, this sub-storm cycle of tail lobe energy storage and release can raise ionospheric currents, which successively lead to geomagnetic induced currents (GICs), a quasi-DC signal, flowing through ground infrastructures like power grids and pipelines [14]. The geomagnetic activity also causes direct and indirect effects; some are health problems, satellite malfunction, and weather change [4]. In addition, space weather can affect today's modern electrical systems and equipment on the Earth, such as navigation, communication, satellite, and power grid systems; as the societal impact of space weather is increasing, operational centers provide a range of predictions for end-users, including geomagnetic storm predictions based on the Kp index [16]. Therefore, the importance of studying geomagnetic storms is twofold; the first one is an academic aspect that is considered as a central part of geophysics, and another one is the practical aspects which in some cases can represent a particular concern for humankind [11].

This paper studied the solar wind parameter by selecting two different geomagnetic events: 27th-29th September 2017 and 25th-27th August 2018. We have applied the cross-correlation technique and wavelet analysis to understand better the fluctuation of solar wind parameters and geomagnetic indices. Understanding solar disturbances on the Earth's magnetic field is aided by measuring geomagnetic changes and related variability [17]. Furthermore, alfvénic fluctuations in the interplanetary Bz factor are closely linked to particle injections [18,19]. This work is presented as follows. Section 2 describes the data sets, followed by the methodology in section 3. Section 4 illustrates the results and discussion, and section 5 concludes the results.

Data set

This present study used an Internet-based supply of data provided by Operating missions as nodes on the internet web system (OMNI). From the OMNI system, we selected data observation of solar wind speed (Vsw), plasma density (Nsw), Plasma temperature (Tsw), and components of an interplanetary magnetic field, Bx, By and Bz, average IMF magnitude (B), and geomagnetic index, the symmetric horizontal component of the geomagnetic field (SYM-H). These data are made readily

available from the official web page of OMNI, https://omniweb.gsfc.nasa.gov/ow.html. The geomagnetic activities were classified as minor, moderate, and severe conditions. These classifications were informed based on National Oceanic and Atmospheric Administration (NOAA) scale.

While the SYM-H index was used to identify the geomagnetic conditions, the space condition during 27th - 29th September 2017 is recognized as a moderate storm, and the condition during 25th - 27th August 2018 is recognized as a relatively intense storm [11]. These events occurred in a descending-to-minimum phase of a solar cycle (SC). Because of the solar cycle period in which it occurred, this solar activity and the resulting space weather effects are vital. From September 27th to 29th, high-speed (defined as Vsw > 550 km/s) streams (HSS) ejected from a positive magnetic field coronal hole (CH32) impacted the Earth's magnetosphere [20]. A CIR has also discovered between 22:48 UT on 26th September and 08:38 UT on 28th September (CIR2). Although no superstorms occurred during this period, the solar and interplanetary scope of this period makes it a convincing analysis that will lead to a deeper understanding of space weather in general. Besides, we have chosen the strong magnetic storm on August 25th–26th, 2018, which occurred at the end of the decline phase of the 24th solar activity cycle with a very low solar flare activity level. Magnetic storms are usually triggered by high-speed solar wind flows from coronal holes during this period of the solar activity cycle; however, coronal mass ejections were responsible for the magnetic storms during the decay of the 24th cycle [21]. A powerful magnetic storm occurred in the Earth's magnetosphere in August 2018 (SYM-H = -206 nT), despite rather mild disturbances on the sun and a low solar wind level. [21]. A more detailed description of the events can be found in Table 1.

Table 1 Events information

Events	Year Month Day/s	Type	Minimum SYM-H Value (nT)	Cause
Event 1	2017 09 27-29	Moderate storm	-74	Corotating interaction region (CIR)
Event 2	2018 08 25-27	Intense storm	-206	Coronal mass ejection (CME)

Methodology

Cross-correlation

Cross-correlation is the function of relative time between the signals, which compares an unknown signal by comparing it with a known signal [22]. In other words, cross-correlation is a statistical tool to measure the similarity between one signal and a time-delayed version of the other signal. Among various parameters, any of them is treated as a known signal, and the rest are treated as an unknown signal. We can calculate the corresponding lead or lag time during the correlation. Researchers (e.g., Dhakal et al. [6], Adhikari et al. [7], Vichare et al. [23]) have mentioned it as the

standard tool for measuring statistical relation among various parameters. The correlation coefficient ranges from -1 to +1, where the bounds indicate maximum correlation and zero indicates no correlation. A high negative correlation indicates a high correlation but the inverse of one series [5,12]. It is one of the best techniques to extent statistical relationships involving various parameters with a function of a time lag [23-25].

Wavelet analysis

Wavelet analysis has been surging as an inclusive technique to scrutinize the non-stationary signals and transform the data, operators, or functions into distinct frequency or scale components [26-28]. The analysis of each part with a scale of analogous resolution depicts that the wavelet is very slender at high frequencies, whereas it is broad at low frequencies. Consequently, wavelet transform is a magnificent tool having time-frequency localization that contemplates momentary high frequencies phenomena.

A continuous wavelet transform (CWT) is one of the most useful mechanisms that enable a continuous description of the signal in a detailed manner, not only in terms of time (t) but also in terms of scale [29]. A scalogram can be used in CWT analysis to evaluate a signal in a time scale plane derived from a square wavelet coefficient module [30]. As a consequence, the data dimension is increased. The signal energy in the wavelet space depicted in the scalogram is conceived using a log2 function that also highlights likewise minor irritations [31]. A more detailed overview of the CWT can be found in Torrence and Compo, 1998 [32]. Through such a study, the time series were seen to have a strong signal and a confidence level of 95%. The CWT approach can be used as an alternative to fix issues including data availability and consistency, database error points, and gaps. Klausner et al. (2013) [33] discussed it in more detail. Mathematically, CWT of a signal x(t) at scale (a) and translation (b) is given by [34]:

$$CWT_x^{(\psi)}(\mathrm{a},\mathrm{b}) = \mathrm{W}(\mathrm{a},\mathrm{b}) = \frac{1}{\sqrt{a}}\int_{-\infty}^{\infty} x(t)\ \Psi^*\left(\frac{t-b}{a}\right)\mathrm{dt} \qquad (1)$$

The results of the CWT are a large number of wavelet coefficients, which are the function of scale (a) and location (b).

We applied this wavelet transform because it is suitable for localizing time and frequency simultaneously. With this in hand, we can analyze the low and high frequency and time period characteristics of the signal. In this paper, the scalograms and the Global Wavelet Spectrum (GWS) have been analyzed to find the variability and periodicity associated with IMF-Bz to withdraw spectral features of geomagnetic activity. Besides three event-specific cases, we have also presented the statistical analysis of periodicities observed in IMF-Bz signals during geomagnetic storms of different intensities. CWT has served as an essential tool to compare the severity of two different kinds of geomagnetic storms under varying space weather conditions.

Results and Discussion

Dynamicity of Interplanetary parameters IMF-Bz, average IMF magnitude (B), solar wind velocity (Vsw), plasma density (Nsw), temperature (Tsw), components of the magnetic field, Bx, By and Bz, and geomagnetic index, SYM-H during two major geomagnetic storms from the 24th Solar cycle was analyzed in this section.

Event 1: 27th – 29th September 2017

Figure 1 represents the variation in interplanetary parameters and geomagnetic indices during a moderate geomagnetic storm on 27th-29th September 2017. A day before the main event day, small amplitude fluctuations have been observed, whereas, on the main event day (28th September 2017), the storm was identified by the sudden commencement on SYM-H index around 00:30 UT. It dropped to a minimum value of -74 nT with local minima of -59 nT around 03:00 UT [35]. The IMF-Bz turns northward and reached -8 nT (Bz < 0) at 5:00 UT due to the influence of incoming energetic charged particles into the magnetosphere [36]. Other solar wind parameter shows a similar variation on 28th September but the event day plasma density reached a value of 9.21 N/cc at 1:00 UT and the subsequent fluctuations were associated with the storm [37]. This is because the plasma density is high near the sun, and as it goes farther, it gradually decreases [38]. Therefore, it has been argued that Solar wind density strongly affects the geomagnetic storm [39-41].

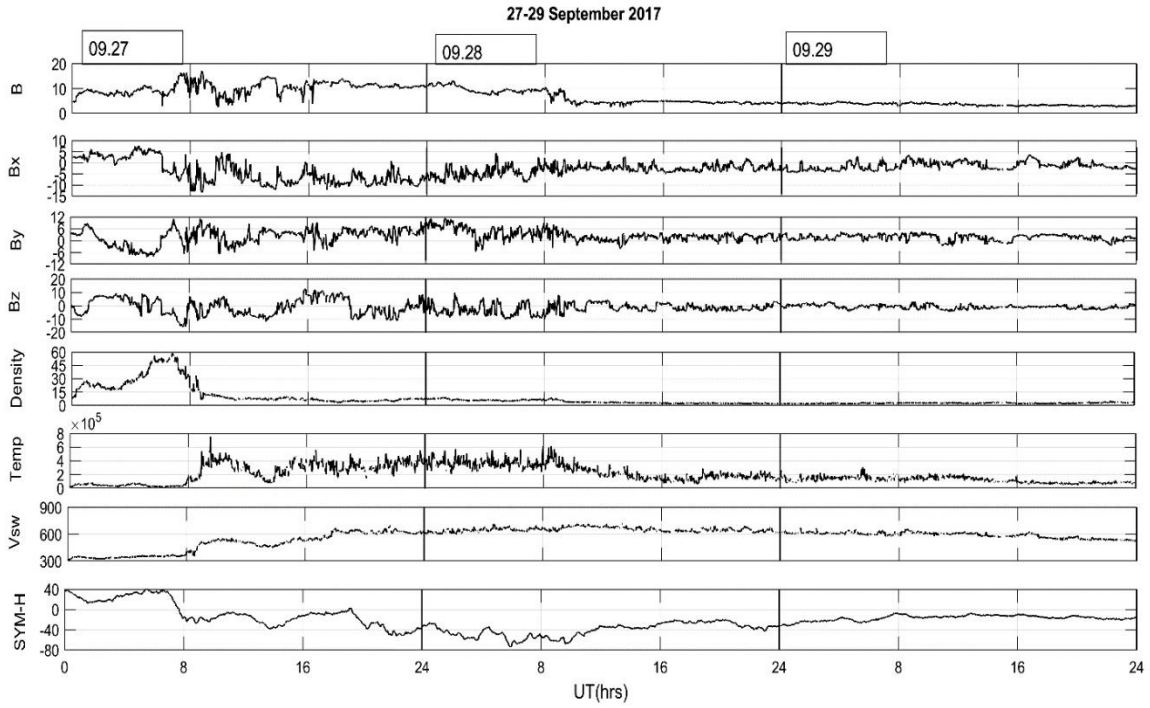

Figure 1 Variation of Interplanetary parameters IMF-Bz (nT), solar wind velocity Vsw (km/s), plasma density Nsw (N/cc), plasma temperature Tsw (K), average IMF magnitude B (nT), components of the magnetic field, Bx (nT), By (nT) and Bz (nT), and geomagnetic index, SYM-H (nT) during 27th – 29th September 2017

Meanwhile, during the event, we can see the abrupt increase of the solar wind speed and plasma temperature with a peak value of ~716 km/s at 10:00 UT and 61.83×10^4 K at 8:00 UT, respectively, on the main event day. Also, the interplanetary magnetic field components B, Bx, and By are observed to have a peak value of 12 nT, -8.85 nT, and -3.17 nT at 00:00 UT, 06:00 UT, and 03:00 UT, respectively. After the event day, all the solar wind parameters show minimal fluctuation, indicating the geomagnetic storm's recovery phase. Concerning the variation on solar wind parameters and geomagnetic indices, we characterized this event as a moderate geomagnetic storm of G3 level according to NOAA weather scale (https://www.swpc.noaa.gov/) [42].

Figure 2 depicts the cross-correlation of SYM-H with Bz (dotted red), Vsw (yellow), Nsw (magenta), Tsw (green), By (blue), B (red), and Bx (black) during the moderate geomagnetic storm of 28th September 2017. The horizontal axis represents the scale from -1500 minutes to +1500 minutes, and the vertical axis represents the cross-correlation coefficients ranging from -1 to +1. The minute averaged SYM-H value has been used as it showed a strong association with solar wind parameters. In the figure, the yellow curve (SYM-H - Vsw), magenta curve (SYM-H – Nsw), green curve (SYM-H – Tsw) depicts a correlation coefficient of -0.98, -0.97, and -0.98, respectively at zero minutes time lag expositing the strong negative correlation of geomagnetic index with Vsw, Nsw, and Tsw when they are in phase. A good negative association of SYM-H and B was reflected by the red curve (SYM-H - B) with a maximum correlation coefficient of -0.98 at +zero minutes lag time, whereas the blue curve (SYM-H - By) shows a maximum negative correlation of -0.77 at zero minutes time lag. Also, the figure reflected the very strong positive correlation of SYM-H and Bx with a cross-correlation coefficient +0.82 at a zero minutes time lag. On the other hand, SYM-H shows a weak positive correlation with Bz (represented by the dotted red line) with a correlation coefficient of +0.20 at zero minutes time lag.

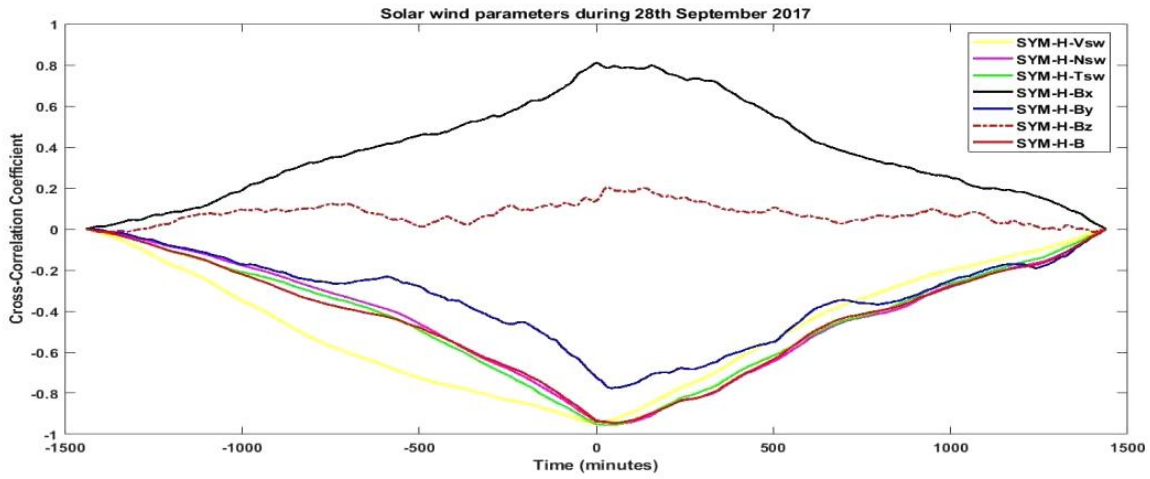

Figure 2 Cross-correlation of SYM-H with H with Bz (dotted red), Vsw (yellow), Nsw (magenta), Tsw (green), By (blue), B (red), and Bx (black) during the moderate geomagnetic storm of 28th September 2017

To study the periodicities of IMF-Bz, we apply wavelet analysis. Figure 3 presents the results of CWT. The peak contours regions seen in the power spectrum comprise a confidence level of more than 95%, which concerns red noise processing levels [43]. Red noise leveling is essential to establish the null hypothesis for the significance of power regions in the wavelet spectrum [1, 7]. We have set the lag 1 autocorrelation coefficient of 0.72 for the construction of red noise. The red dotted line in GWS (Figure 3(c)) corresponds to the red noise spectrum.

The vertical plane in the scalogram (Figure 3(b)) is the time in minutes, and the horizontal plane is the period in the minutes. Dealing with finite-length time series makes an error occur at the edges of the wavelet power spectrum [7]. To overcome this, we padded the time series with appropriate zeros. However, adding zeros creates discontinuities at the edges of the time series, which is solved by inserting a cone of influence (represented in the figures with U-shaped black lines). The edge effects are negligible beyond the cone of influence [44].

The peaks observed in the GWS plot show the main periodicities associated with the IMF-Bz fluctuations during the main phase of the geomagnetic storm of 28th September 2017. From the scalogram in Figure 3, it is evident that the abrupt changes in the magnetic field show a significant periodicity of 128 minutes in the regions 200 - 500 minutes. We found high wavelet power on the global power continuum corresponding to a critical periodicity of 128 minutes with energy ~450 unit^2. It resembles the results of time series analysis with better visualization of the frequency content.

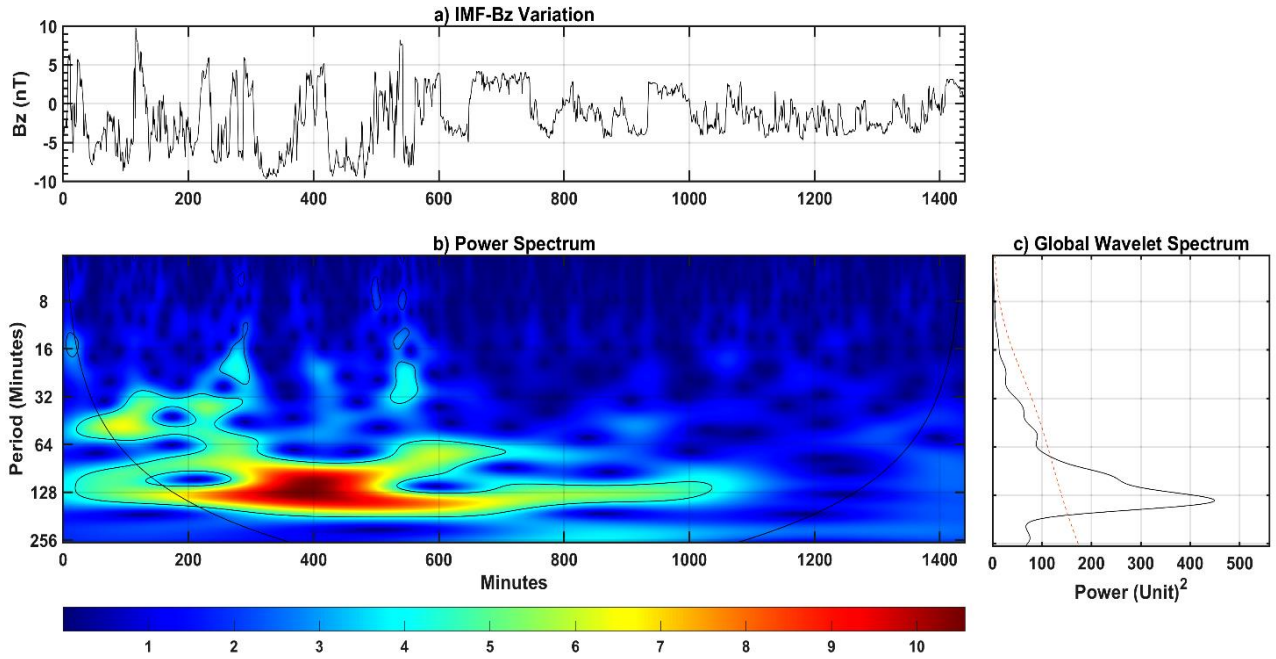

Figure 3 (a) IMF-Bz variation during a moderate geomagnetic storm event (occurred on 28th September 2017), (b) Scalogram of Bz for moderate geomagnetic storm event occurring on 28th September 2017, and (c) Global wavelet spectrum of Bz for moderate geomagnetic storm event (occurred on 28th September 2017)

Event 2: 25th – 27th August 2018

Figure 4 represents the variation in interplanetary solar wind parameters obtained from OMNI data during the geomagnetic event of 25th – 27th August 2018. Basically, it shows the fluctuations of the interplanetary parameters, B, Bx, By, Bz, Vsw, Nsw, Tsw, and geomagnetic index, SYM-H. It is evident that the shock associated with the geomagnetic storm was marked by the significant fluctuations on IMF-Bz along N-S direction on 26th August 2018. IMF-Bz turned northward and reached a value of -16.22 nT at 05:00 UT that triggers some geomagnetic activities [1, 29]. Similarly, the SYM-H index dropped to -206 nT at its lowest around 07:00 UT resulting from the variation in southward interplanetary magnetic field IMF (Bz < 0). It accounts for the energy injection process from the solar wind particles into the magnetosphere [35, 36, 45]. Meanwhile, the solar wind stream peaked with an average value of 427 km/s at 16:00 UT before the initial phase of the solar storm, and later it increased to 547.4 km/s around 23:00 UT. Also, solar wind proton density suddenly shows an increment during the main phase of the geomagnetic storm. It gradually decreases from the late hours of the event day (26th August), and the solar wind temperature fluctuates considerably, reaching ~42.4756 × 10^4 K at 18:00 UT during the main phase of the geomagnetic storm. The B component reached 4.44 nT at 20:00 UT and peaked at 19.12 nT around 09:00 UT.

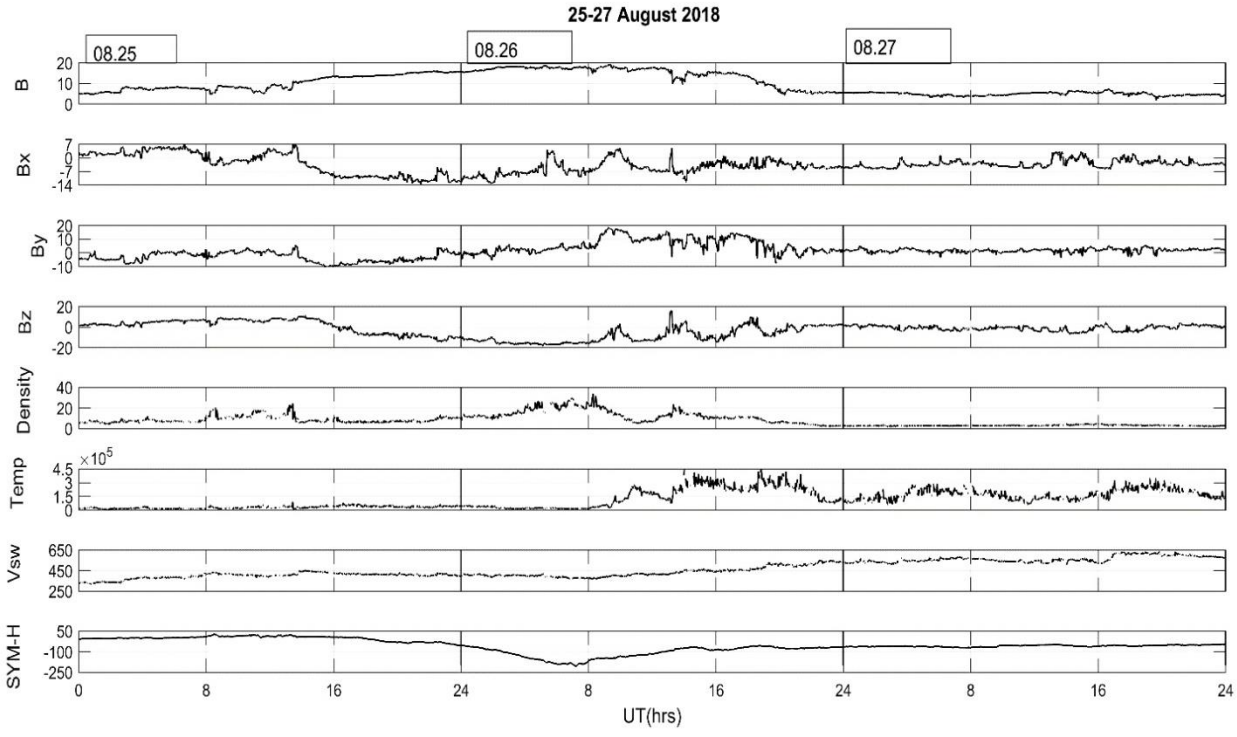

Figure 4 Cross-correlation of SYM-H with H with Bz (dotted red), Vsw (yellow), Nsw (magenta), Tsw (green), By (blue), B (red), and Bx (black) during the moderate geomagnetic storm of 28th September 2017

Similarly, the By and Bx component are observed to have peak values of −9.09 nT at 13:00 UT and -12.01 nT at 14:00 UT, respectively. Therefore, temperature, composition, and ionospheric circulation parameters can change due to the energy injection mechanism inside the magnetosphere and ionosphere during geomagnetic disturbances [11,46]. Regarding the values of geomagnetic indices and solar wind parameters, the geomagnetic event of 25th – 27th August 2018 was considered the intense geomagnetic storm of the G4 level according to NOAA weather scale (https://www.swpc.noaa.gov/) [42].

Figure 5 depicts the cross-correlation of SYM-H with Bz (dotted red), Vsw (yellow), Nsw (magenta), Tsw (green), By (blue), B (red), and Bx (black) during the moderate geomagnetic storm of 28th September 2017. The cross-correlation technique has been applied to measure the similarity pattern information between two-time series signals [12,22,45]. In the figure, the yellow curve (SYM-H - Nsw), magenta curve (SYM-H – Vsw), green curve (SYM-H – B) depicts a correlation coefficient of -0.96, -0.86, and -0.96, respectively, at a zero-time lag. This suggests that Nsw, B, and Vsw are highly and negatively correlated with the SYM-H index when they are in phase. The SYM-H – By (blue curve) and SYM-H - Tsw (green curve) show a maximum negative correlation of -0.89 at -36 minutes and -552 minutes lag time, describing the strong negative association. The curve reaching the vicinity of +1 explains the highest correlation in the cross-correlation plot [47]. A good positive association of Bx and Bz with SYM-H was reflected by the black curve (SYM-H - Bx) and dotted red (SYM-H – Bz) with a maximum correlation coefficient of +0.78 and +0.75 at a time lag of -176 minutes and -230 minutes, respectively. Even though IMFBz is not a necessary condition for causing a geomagnetic storm in most situations, this higher magnitude of correlation coefficient may have occurred due to the significant role played by IMFBz for the injection of energetic particles in this particular event. Nonetheless, Gonzalez et al. [11] and Gonzalez and Tsurutani [48] suggested that a sufficiently high IMF-Bz could be sufficient to cause geomagnetic disturbances. The greater value of lags suggests that the response time for a geomagnetic storm is longer to inject particles into the ring current region [49].

Figure 6 represents the result of the CWT for the intense geomagnetic event of 26th August 2018. In this figure, the strong power regions corresponding to Bz's peaks in the global wavelet spectrum were observed between the periods 128-256 minutes. As depicted by the global wavelet spectrums in Figure 6(c), the most significant periodicity of 256 minutes was observed with corresponding energy ~3800 unit2. Besides, a small part of thick power regions lies outside the cone of influence, losing its significance (Figure 6(b)). In general, the wavelets keep soundtrack of the high-frequency details (abrupt changes in the interplanetary magnetic field) for the entire study period. A similar type of analysis can also be found in [7,34,50]. It is not surprising that this result presents the scope of CWT as a vital tool for providing information about the frequencies of the event and its location in the time series under different geomagnetic conditions.

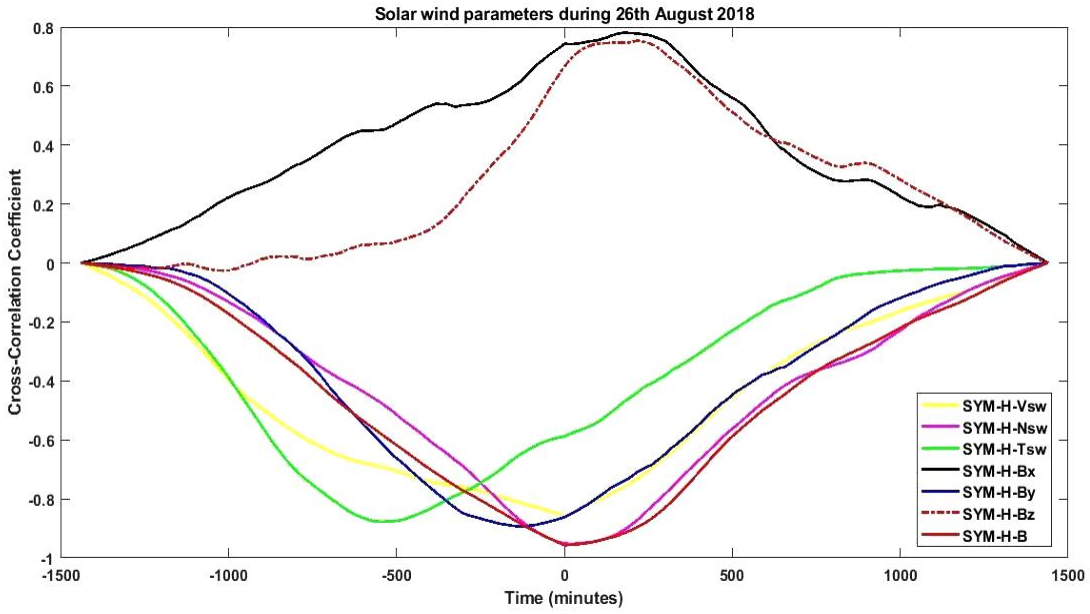

Figure 5 *Cross-correlation of SYM-H with Bz (dotted red), Vsw (yellow), Nsw (magenta), Tsw (green), By (blue), B (red), and Bx (black) during the moderate geomagnetic storm of 26th August 2018*

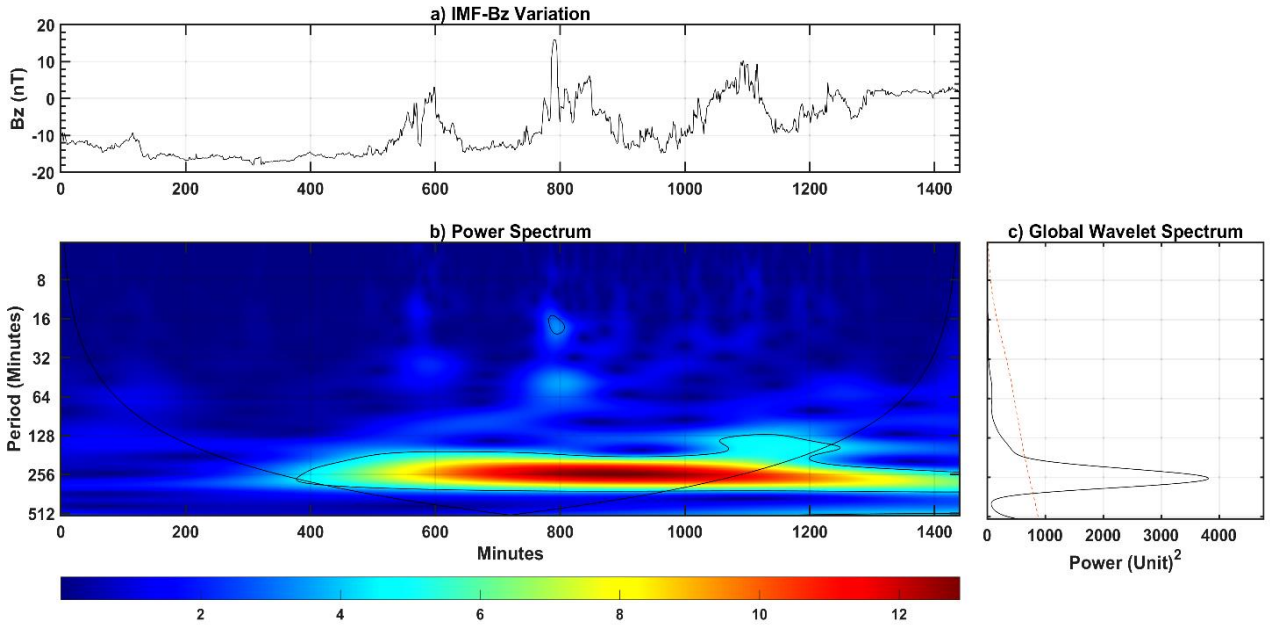

Figure 6 *(a) IMF-Bz variation during an intense geomagnetic storm event (occurred on 26th August 2018), (b) Scalogram of Bz for an intense geomagnetic storm event, and (c) Global wavelet spectrum of Bz for the intense geomagnetic storm event*

Conclusion

This paper concisely presented a detailed study of various solar wind parameters and geomagnetic indices using OMNI data for two different geomagnetic events, 27th – 29th September 2017 and 25th – 27th August 2018. The study of a geomagnetic storm is an essential issue for the study of space weather. The Bz component is an important parameter that indicates the presence of a geomagnetic storm. The time-series analysis of the OMNI parameters (solar wind parameters and geomagnetic indices) presented the significant changes on these parameters associated with different phases of the geomagnetic storm. Our study observes that events 1 and 2 show varying effects on the space weather environment described based on the Gonzalez et al. [11] and have the Bz value -8 nT and -16.22 nT, respectively. During a geomagnetic disturbance, there is an energy input inside the magnetosphere, which changes atmospheric parameters, such as the composition and temperature of the atmospheric particles. The induced disturbances also depend upon the strength of the geomagnetic storm.

Cross-correlation analysis presented the dependence of geomagnetic index (SYM-H) value with solar wind parameters. For both events, the SYM-H value shows a strong negative association with Vsw, Nsw, Tsw, By, and B. On the other hand, a good positive association of SYM-H with B was noticed. Meanwhile, we also noted that the IMF-Bz strongly correlates with SYM-H on an intense storm day rather than the moderate geomagnetic period. We conducted a wavelet transformation of the IMF-Bz time series to study the periodicity in the interplanetary magnetic field component, Bz, particularly on the main event day. By manually examining the power spectrum of each case, the IMF-Bz values are found to exhibit a typical periodicity of ~128 - 256 minutes. The associated variations in IMF-Bz, however, differ with the intensity of the geomagnetic storms. In general, we noticed that cross-correlation and CWT results point to the fact that these approaches provide an alternative way of assessing the global effects of a geomagnetic storm on the solar wind parameters and geomagnetic indices and could be used as a sophisticated tool to forecast the emergence of these unique events. Combining the measurements from different geomagnetic storms, we can mitigate disturbances related to radio signal propagation, power grid fluctuations and widespread voltage control problems in the power systems, induced pipeline currents, orientation problems in the satellite operation by tracking the solar activities and the ionospheric response during the several solar events.

References

[1] B. Adhikari, B. Kaphle, N. Adhikari, S. Limbu, A. Sunar, R. K. Mishra and S. Adhikari, “Analysis of cosmic ray, solar wind energies, components of Earth’s magnetic field, and ionospheric total electron content during solar superstorm of November 18–22, 2003”, SN Applied Sciences, 1, 453 (2019).

[2] I. G. Richardson, “Coronal mass ejections and their sheath regions in interplanetary space”, Living Reviews in Solar Physics, 15, 1 (2018).

[3] E. N. Parker, “Dynamics of the interplanetary gas and magnetic fields”, Astrophysical Journal, 128, 664 (1958).

[4] A. Silwal, S. P. Gautam, N. P. Chapagain, M. Karki, P. Poudel, B. D. Ghimire, R. K. Mishra, B. Adhikari, “Ionospheric Response over Nepal during the 26 December 2019 Solar Eclipse”, Journal of Nepal Physical Society, 7, 25-30 (2021).

[5] A. Silwal, S. P. Gautam, P. Poudel, M. Karki, B. Adhikari, N. P. Chapagain, R. K. Mishra, B. D. Ghimire, Y. Migoya-Orue, “GPS Observations of Ionospheric TEC Variations during the 15th Jan 2010 and 21st June 2020 Solar Eclipse”, *Radio Science*, 56, (2021).

[6] S. Dhakal, B. Adhikari, K. Pudasainee, N. P. Chapagain, D. Pandit, S. Dahal, B. Shrestha, B. Sapkota, and D. N. Chhatkuli, “Correlation of solar wind velocity with different parameters during geomagnetic disturbances”, BIBECHANA, 16, 165-176 (2019).

[7] B. Adhikari, N. Sapkota, B. Bhattarai, R. K. Mishra, S. Bohora, N. P. Chapagain and B. Regmi, “Study of interplanetary parameters, polar cap potential, and polar cap index during the quiet event and high-intensity long-duration continuous AE activities (HILDCAAs)”, Russian Journal of Earth Sciences, 18, ES1001 (2018).

[8] A. Bhaskar and G. Vichare, “Forecasting of SYMH and ASYH indices for geomagnetic storms of solar cycle 24 including St. Patrick's Day, 2015 storm using NARX neural network”, Journal of Space Weather and Space Climate, 9, A12 (2019).

[9] J. A. Wanliss and K. M. Showalter, “High-resolution global storm index: Dst versus SYM-H”, Journal of Geophysical Research-Atmospheres, 111, A02202 (2006).

[10] A. Dal Lago, L. E. A. Vieira, E. Echer, W. D. Gonzalez, A. L. Clúa de Gonzalez, F. L. Guarnieri, L. Balmaceda, J. Santos, M. R. da Silva, A. de Lucas and N. J. Schuch, “Great geomagnetic storms in the rise and maximum of solar cycle 23”, Brazilian Journal of Physics, 34, 1542-1546 (2004).

[11] W. D. Gonzalez, J. A. Joselyn, Y. Kamide, H. W. Kroehl, G. Rostoker, B. T. Tsurutani, V. M. Vasyliunas, “What is a geomagnetic storm?”, Journal of Geophysical Research, 99, 5771-5792 (1994).

[12] B. Adhikari, P. Baruwal and N. P. Chapagain, "Analysis of supersubstorm events with reference to polar cap potential and polar cap index", Earth and Space Science, 4, 2-15 (2017).

[13] B. B. Rana, N. P. Chapagain, B. Adhikari, D. Pandit, K. Pudasainee, Shaswat Chapagain and D. N. Chhatkuli, “Study of total electron content and electron density profile from satellite observations during geomagnetic storms”, Journal of Nepal Physical Society, 5, 59-66 (2019).

[14] C. Haines, M. J. Owens, L. Barnard, M. Lockwood and A. Ruffenach, “The variation of geomagnetic storm duration with intensity”, Solar Physics, 294, 154 (2019).

[15] D. N. Baker, “What is space weather?”, Advances in Space Research, 22, 7 (1998).

[16] S. Chakraborty and S. K. Morley, “Probabilistic prediction of geomagnetic storms and the Kp index”, Journal of Space Weather and Space Climate, 10, 36 (2020).

[17] E. O. Falayi and A. B. Rabiu, “Dependence of time derivative of horizontal geomagnetic field on sunspot number and aa index”, Acta Geophysica, 61, 211-222 (2013).

[18] H. J. Kim, D. Y. Lee and L. R. Lyons, “Are repetitive particle injections during high-speed solar wind streams classic substorms?”, Journal of Geophysical Research, 113, A0820 (2008).

[19] M. I. Sandanger, F. Søraas, K. Aarsnes, K. Oksavik, D. S. Evans and M. S. Greer, "Proton injections into the ring current associated with Bz variations during HILDCAA events", In T. I. Pulkkinen, N. A. Tsyganenko and R. H. W. Friedel (Eds.), The inner magnetosphere: Physics and modeling, Geophysical Monograph, Washington DC, USA: American Geophysical Union, 155, 249-255 (2005).

[20] R. Hajra, B. T. Tsurutani and G. S. Lakhina, "The complex space weather events of 2017 September", Astrophysical Journal, 899, 3 (2020).

[21] N. G. Kleimenova, L. I. Gromova, S. V. Gromov and L. M. Malysheva, "The magnetic storm of August 25–26, 2018: Dayside high latitude geomagnetic variations and pulsations", Geomagnetism and Aeronomy, 59, 660-667 (2019).

[22] A. E. Usoro, "Some basic properties of cross-correlation functions of n-dimensional vector time series", Journal of Statistical and Econometric Methods, 4, 63-71 (2015).

[23] G. Vichare, S. Alex and G. S. Lakhina, "Some characteristics of intense geomagnetic storms and their energy budget", Journal of Geophysical Research, 110, A03204 (2005).

[24] P. Poudel, N. Parajuli, A. Gautam, D. Sapkota, H. Adhikari, B. Adhikari, A. Silwal, S. P. Gautam, M. Karki, R. K. Mishra, "Wavelet and cross-correlation analysis of relativistic electron flux with sunspot number, solar flux, and solar wind parameters", Journal of Nepal Physical Society, 6, 104-112 (2020).

[25] A. J. Mannucci, B. T. Tsurutani, M. A. Abdu, W. D. Gonzalez, A. Komjathy, E. Echer, B. A. Iijima, G. Crowley and D. Anderson, "Superposed epoch analysis of the dayside ionospheric response to four intense geomagnetic storms", Journal of Geophysical Research, 113, A00A02 (2008).

[26] G. Strang and T. Nguyen, "Wavelet and filters banks", Cambridge: Wellesley-Cambridge press (1996).

[27] E. K. Foufoula-Georgiou and P. Kumar, "Wavelet in geophysics", New York: Academic Press (1995).

[28] O. Mendes, M. O. Domingues, A. M. da Costa and A. L. Clúa de Gonzalez, "Wavelet analysis applied to magnetograms: Singularity detections related to geomagnetic storms", Journal of Atmospheric and Solar-Terrestrial Physics, 67, 1827-1836 (2005).

[29] B. Adhikari, P. Poudel, S. Simkhada, D. Sharma and J. J. Nakarmi, "Variation of solar wind parameters along with the understanding of energy dynamics within the magnetospheric system during geomagnetic disturbances", Earth and Space Science, 6, 276-293 (2019).

[30] J. P. Antoine, R. P. V. Murenzi and S. T. Ali, "Two-dimensional wavelets and their relatives", Cambridge: Cambridge University Press (2008).

[31] J. Morlet, "Sampling theory and wave propagation", In Issues in acoustic signal/Image processing and recognition, New York: Springer-Verlag, 1, 233–261 (1983).

[32] C. Torrence and G. P. Compo, "A practical guide to wavelet analysis", Bulletin of the American Meteorological Society, 79, 61–78 (1998).

[33] V. Klausner, E. A. Kherani and M. T. A. H. Muella, "Near- and far-field tsunamigenic effects on the Z component of the geomagnetic field during the Japanese event, 2011", Journal of Geophysical Research: Space Physics, 121, 1772-1779 (2016).

[34] V. Klausner, M. O. Domingues, O. Mendes, A. R. R. Papa and P. Frick, "Characteristics of solar diurnal variations: a case study based on records from the ground magnetic observatory at Vassouras, Brazil", Space Physics, arXiv:1210.1768v1 [physics.space-ph] (2012).

[35] B. T. Tsurutani, W. D. Gonzalez, F. Tang, S. I. Akasofu and E. J. Smith, "Origin of interplanetary southward magnetic fields responsible for major magnetic storms near solar maximum (1978–1979)", Journal of Geophysical Research, 93, 8519 (1988).

[36] J. F. Lemaire, "The effect of a southward interplanetary magnetic field on Stormer's allowed regions", Advances in Space Research, 31, 1131-1153 (2012).

[37] L. M. Celnikier, L. Muschietti and M. V. Goldman, "Aspects of interplanetary plasma turbulence", Astronomy & Astrophysics, 181, 138-154 (1987).

[38] J. T. Gosling, P. Riley, D. J. McComas and V. J. Pizzo, "Over expanding coronal mass ejections at high heliographic latitudes: Observations and simulations", Journal of Geophysical Research, 103, 1941-1954 (1998).

[39] R. S. Weigel, "Solar wind density influence on geomagnetic storm intensity", Journal of Geophysical Research, 115, A09201 (2010).

[40] J. G. Wu and H. Lundstedt, "Geomagnetic storm predictions from solar wind data with the use of dynamic neural networks", Journal of Geophysical Research, 102, 14255-14268 (1997).

[41] T. P. O'Brien and R. L. McPherron, "Evidence against an independent solar wind density driver of the terrestrial ring current", Geophysical Research Letters, 27, 3797-3800 (2000).

[42] Space Weather Prediction Center, National Oceanic and Atmospheric Administration, "Space weather conditions on NOAA scales", from https://www.swpc.noaa.gov/.

[43] C. Katsavrias, P. Preka-Papadema and X. Moussas, "Wavelet analysis on solar wind parameters and geomagnetic indices", Solar Physics, 280, 623-640 (2012).

[44] K. Khanal, B. Adhikari, N. P. Chapagain and B. Bhattarai, "HILDCAA-related GIC and possible corrosion Hazard in underground pipelines: A comparison based on wavelet transform", Space Weather, 17, 238-251 (2019).

[45] B. Adhikari, S. Dahal and N. P. Chapagain, "Study of field-aligned current (FAC), interplanetary electric field component (Ey), interplanetary magnetic field component (Bz), and northward (x) and eastward (y) components of the geomagnetic field during supersubstorm", Earth and Space Science, 4, 257-274 (2017).

[46] W. D. Gonzalez, B. T. Tsurutani, A. L. Clua-Gonzalez, "Interplanetary origin of geomagnetic storms", Space Science Reviews, 88, 529-562 (1999).

[47] R. W. Katz, "Use of cross-correlations in the search for teleconnections", Journal of Climatology, 8, 241-253 (1988).

[48] B. T. Tsurutani and W. D. Gonzalez, "The cause of High-Intensity Long-Duration continuous AE Activity (HILDCAAS): Interplanetary Alfven wave trains", Planetary and Space Science, 35, 405-412 (1987).

[49] I. A. Daglis, R. M. Thorne, W. Baumjohann and S. Orsini, "The terrestrial ring current: Origin, formation and decay", Reviews of Geophysics, 37, 407-438 (1999).

[50] A. Marques de Souza, E. Echer, M. J. A. Bolzan, R. Hajra, "Cross-correlation and cross-wavelet analyses of the solar wind IMF B z and auroral electrojet index AE coupling during HILDCAAs", In *Annales Geophysicae*, 36, 205-211 (2018).